Structure
Article

Structural Basis for Calmodulin as a Dynamic Calcium Sensor

Miao Zhang,[1] Cameron Abrams,[5] Liping Wang,[1] Anthony Gizzi,[1] Liping He,[1] Ruihe Lin,[1] Yuan Chen,[1,6] Patrick J. Loll,[4] John M. Pascal,[3] and Ji-fang Zhang[1,2,*]
[1]Department of Molecular Physiology and Biophysics
[2]Farber Institute for Neurosciences and Graduate Program in Neuroscience
[3]Department of Biochemistry
Jefferson Medical College, 1020 Locust Street, Philadelphia, PA 19107, USA
[4]Department of Biochemistry and Molecular Biology, College of Medicine, Drexel University, Philadelphia, PA 19102, USA
[5]Department of Chemical and Biological Engineering, Drexel University, Philadelphia, PA 19104, USA
[6]Present address: Center of Neurosciences, Zhongshan Medical School of Sun Yat-sen University, 74 Zhongshan Road II Guangzhou, Guangdong 510080, People's Republic of China
*Correspondence: ji-fang.zhang@jefferson.edu
DOI 10.1016/j.str.2012.03.019

SUMMARY

Calmodulin is a prototypical and versatile Ca^{2+} sensor with EF hands as its high-affinity Ca^{2+} binding domains. Calmodulin is present in all eukaryotic cells, mediating Ca^{2+}-dependent signaling. Upon binding Ca^{2+}, calmodulin changes its conformation to form complexes with a diverse array of target proteins. Despite a wealth of knowledge on calmodulin, little is known on how target proteins regulate calmodulin's ability to bind Ca^{2+}. Here, we take advantage of two splice variants of SK2 channels, which are activated by Ca^{2+}-bound calmodulin but show different sensitivity to Ca^{2+} for their activation. Protein crystal structures and other experiments show that, depending on which SK2 splice variant it binds to, calmodulin adopts drastically different conformations with different affinities for Ca^{2+} at its C-lobe. Such target protein-induced conformational changes make calmodulin a dynamic Ca^{2+} sensor capable of responding to different Ca^{2+} concentrations in cellular Ca^{2+} signaling.

INTRODUCTION

As the prototypical Ca^{2+} sensor, calmodulin (CaM) is widely expressed in all eukaryotic cells, mediating a variety of cellular signaling processes, including regulation of enzymatic activities, modulation of ion channel activities, synaptic transmission and plasticity, and regulation of gene expression (Clapham, 2007; Deisseroth et al., 1998; Dick et al., 2008; Drum et al., 2002; Halling et al., 2005; McLaughlin and Murray, 2005; Wayman et al., 2008; Xia et al., 1998; Zühlke et al., 1999). A diverse array of target proteins has been identified, such as CaM kinases and ion channels, which are known to interact with CaM with or without Ca^{2+}. CaM is also a versatile Ca^{2+} sensor, capable of responding to a wide range of Ca^{2+} concentrations (10^{-12} M–10^{-6} M) in Ca^{2+}-dependent signal transduction (Chin and Means, 2000). Four canonical EF hands, two located at the CaM N terminus (N-lobe) and the other two at the C terminus (C-lobe), serve as the high-affinity Ca^{2+} binding motifs (Meador et al., 1992, 1993). The N- and C-lobes are connected by an extremely flexible central linker region. EF hands at the C-lobe are generally thought to have a higher affinity for Ca^{2+} than those in the N-lobe (Andersson et al., 1983; Crouch and Klee, 1980). Upon binding Ca^{2+}, CaM changes its conformation from the closed configuration to the open one, exposing the hydrophobic surfaces within the N- and C-lobes for Ca^{2+}-dependent interactions with the target proteins (Chin and Means, 2000; Halling et al., 2005; Hoeflich and Ikura, 2002; Ikura et al., 1992; Ishida and Vogel, 2006; Kranz et al., 2002; Meador et al., 1992, 1993; Schumacher et al., 2004). Additional conformational changes—most noticeably, unwinding of the α helix of the CaM linker region (R74 to E83) to various degrees—allow CaM to adopt different conformations in its interactions with different target proteins, ranging from the compact (collapsed) conformation to its full extended conformation (Drum et al., 2002; Fallon and Quiocho, 2003; Ikura et al., 1992; Meador et al., 1992, 1993; Mori et al., 2008; Van Petegem et al., 2005).

Such structural flexibility explains how CaM is capable of interacting with target proteins with distinct structural features (Halling et al., 2005; Ishida and Vogel, 2006). So far, most structural studies have focused on how binding of Ca^{2+} to CaM exposes the hydrophobic surfaces for interaction with target proteins. Despite a wealth of knowledge on CaM, much less is known about how CaM's affinity for Ca^{2+} is determined, in particular, how binding of CaMBDs can reciprocally affect CaM's conformations and, consequently, change CaM's affinities for Ca^{2+}. It is generally thought that formation of CaM-target protein complexes increases CaM's affinity for Ca^{2+}. Furthermore, it is also less clear how regulation of CaM's affinity for Ca^{2+} by target proteins is achieved at the molecular level. This knowledge gap is, in part, due to technical difficulties, such as the size limitation of proteins used in nuclear magnetic resonance experiments or the challenges of getting protein crystals of CaM complexed with bigger target proteins. Consequently, short CaMBD peptides (typically 15-mers to 30-mers) are often used in structural studies, and they are often too short to produce any significant impact on CaM's conformations.

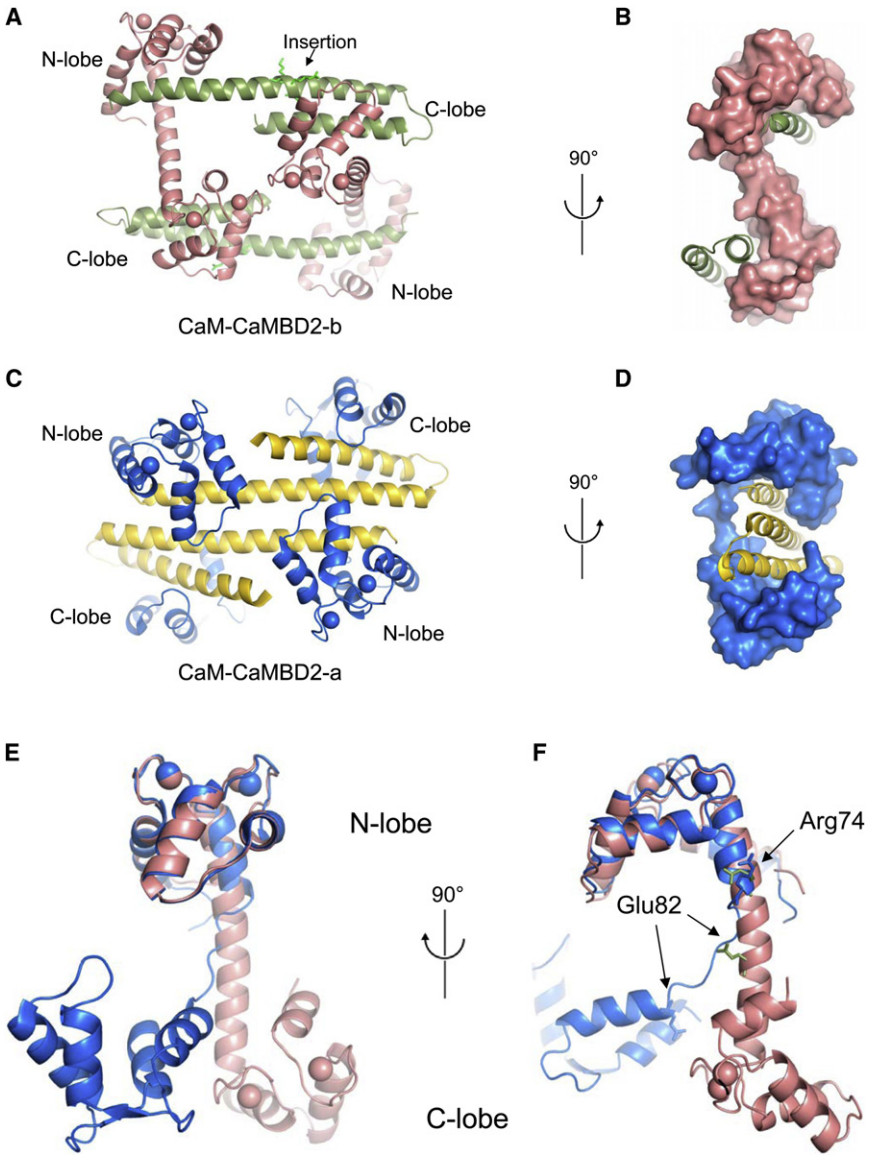

Figure 1. A Distinct Conformation of the CaM-CaMBD2-b Complex

(A and B) Structure of the CaM-CaMBD2-b complex. A 2×2 complex is formed with two horizontal CaMBD2-b peptides, in green, and two CaM molecules, in salmon pink (A). Also shown are side chains of the three residues A463, R464, and K465 in CaMBD2-b. A 90° turn of the structure shows that CaM in CaMBD2-b adopts an "S"-shaped configuration (B).

(C and D) Structure of the CaM-CaMBD2-a complex (1G4Y). Two CaMBD2-a peptides, in gold, and two CaM molecules, in blue, form the 2×2 complex (C). CaM in the CaM-CaMBD2-a complex displays a "C"-like structure (D).

(E and F) Comparison of the structures of CaM from CaM-CaMBD2-b (in salmon pink) and CaM-CaMBD-2a (in blue). The CaM structures are aligned at the N-lobe. Notice the difference at the linker region (R74-E82).

See also Figure S1.

Small-conductance Ca^{2+}-activated potassium channels (SK) are widely expressed in brain and play pivotal roles in regulating neuronal excitability, dendritic integration, and synaptic transmission (Faber, 2009; Köhler et al., 1996; Stocker, 2004). Activation of SK is achieved exclusively by intracellular Ca^{2+} (Xia et al., 1998). CaM, constitutively tethered to SK, serves as the high-affinity Ca^{2+} sensor. Binding of Ca^{2+} to CaM, particularly at the N-lobe, changes the channel conformation and opens the channel (Schumacher et al., 2004, 2001). Activation of SKs is highly sensitive to Ca^{2+} with a half maximal effective concentration (EC_{50}) around 300 – 700 nM (Köhler et al., 1996; Xia et al., 1998). Three SK genes have been identified, *KCNN1*, *KCNN2*, and *KCNN3* (Bond et al., 2005). We have recently identified an SK2 splice variant, SK2-b, which is less sensitive to Ca^{2+} for its activation, compared to the original SK2 channel, SK2-a (L.H. and J.F.Z., unpublished data). These two SK2 splice variants are virtually identical in their primary amino acid sequence with the exception that SK2-b has three additional amino acid residues—A463, R464, and K465 (ARK)—in its CaMBD.

Since SK channels are exclusively activated by Ca^{2+}-bound CaM, this pair of SK2 splice variants provides a unique experimental model for us to test how target proteins may regulate the CaM's ability to bind Ca^{2+}. We have determined the X-ray crystal structure of CaM complexed with CaMBD from SK2-b (CaMBD2-b) at a resolution of 1.9 Å and compared to the previously determined structure of CaM-CaMBD2-a (Schumacher et al., 2001). Along with biochemical, biophysical, and electrophysiological data, we demonstrate that the structural flexibility of CaM occurs not only at the CaM linker region but also extensively in its hydrophobic interfaces, induced by these two CaMBDs. Our results provide direct experimental evidence supporting the notion that target proteins can change the conformation of CaM and, more important, regulate the affinity of CaM for Ca^{2+}, thus making CaM a dynamic Ca^{2+} sensor capable of responding to a wide range of Ca^{2+} concentrations in cellular Ca^{2+} signal transduction.

RESULTS

Structure of the CaM-CaMBD2-b Complex

To explore how target proteins may affect the affinity of CaM for Ca^{2+}, we determined the X-ray crystal structure of the CaM-CaMBD2-b complex in the presence of Ca^{2+} at a resolution of 1.9 Å (Figure 1; Figure S1 available online; Table 1). The CaM-CaMBD2-b complex shows a 2×2 architecture, with two CaMs (vertical) and two CaMBD2-b peptides (horizontal) in an antiparallel arrangement (Figures 1A and 1C). Both CaMBD2-b and CaMBD2-a adopt the same hairpin α-helical structure (Figures

Table 1. Crystallographic Statistics

	CaM-CaMBD2-b complex
Data collection	
Space group	P1
Unit cell dimensions	a = 47.7 Å, b = 65.6 Å, c = 66.1 Å
	α = 90.7°, β = 110.5°, γ = 111.0°
Wavelength (Å)	1.075
Resolution range (Å)	30–1.9 (2.0–1.9)
Completeness (%)	97.9 (96.1)
Total observations	620,836 (77,935)
Unique observations	53,499 (7,715)
Mean redundancy	11.6 (10.1)
Mean I/σ(I)	15.6 (2.6)
R_{merge}[a]	0.093 (0.936)
R_{pim}[b]	0.030 (0.325)
Model refinement	
Resolution range (Å)	20–1.9 (1.97–1.9)
Number of reflections	53,458 (4,945)
R_{work}[c]	0.170 (0.242)
R_{free}[c]	0.195 (0.288)
Number of atoms/average B factor (Å^2)	4,123/43.9
Protein	3,687/42.0
Calcium ions	8/31.0
Solvent	318/49.6
Ligands (glycerol, sulfate, phenylurea)	110/58.2
Phi/psi, most favored (%)	99.3
rmsd bond angles (°)	0.885
rmsd bond lengths (Å)	0.013

Values in parentheses refer to data in the highest resolution shell. rmsd, root-mean-square deviation.
[a] $R_{merge} = \Sigma_{hkl}\Sigma_j|I_j - \langle I\rangle|/\Sigma_{hkl}\Sigma_j I_j$. $\langle I\rangle$ is the mean intensity of *j* observations of reflection *hkl* and its symmetry equivalents.
[b] R_{pim} (precision-indicating merge) = $\Sigma_{hkl}(1/n_{hkl} - 1)^{1/2}\Sigma_j|I_j - \langle I\rangle|/\Sigma_{hkl}\Sigma_j I_j$. n, number of observations of reflection hkl.
[c] $R_{cryst} = \Sigma_j|F_{obs} - kF_{calc}|/\Sigma_{hkl}|F_{obs}|$. R_{free} = R_{cryst} for 5% of reflections excluded from crystallographic refinement.

1A and 1C). Insertion of ARK does not disrupt the propensity of CaMBD2-b to form α-helix (Figures 1A and S1D), nor are there any direct contacts between ARK and the CaM hydrophobic interfaces (Figure 1A), where Ca^{2+}-dependent interactions between CaM and its target proteins typically take place, although R464 forms a salt bridge with E120 of CaM outside of the hydrophobic interfaces. In both complexes, the CaM N-lobe interacts with the C-terminal fragment of the CaMBD peptide, whereas the C-lobe interacts with the N-terminal fragment of the CaMBD peptide. Compared to CaM-CaMBD2-a, the structure of the CaM-CaMBD2-b complex shows distinct features, particularly the CaM conformation (Figure 1).

Overall, significant differences exist in the CaM structure between CaM-CaMBD2-b and CaM-CaMBD2-a (root-mean-square deviation [rmsd] = 12.16 Å). Such differences, however, are not spread uniformly across the entire CaM. The CaM N-lobe from both complexes displays nearly identical structure, with rmsd = 0.86 Å. In contrast, the CaM C-lobe shows dramatic differences between the two complexes (rmsd = 2.53 Å). A significant difference is also seen in the CaM linker region (rmsd = 4.83 Å; Figures 1E and 1F). The CaM linker region in our model maintains a rigid α-helix, leading to approximately a 180° rotation of the C-lobe (Figures 1E and 1F). Consequently, CaM in our structure adopts an "S"-like configuration (Figures 1B and 1F). In comparison, the CaM linker region in CaM-CaMBD2-a unfolds from R74 to E82, resulting in a moderate collapse of CaM and, thus, a "C"-like configuration (Figures 1D and 1F). Comparison was also made between our structure and that of the CaM-edema-factor complex (1K90; Figure S1E). In the latter complex, the CaM linker region unwinds within a much shorter span of the α-helix. Another obvious difference is in how CaMBDs are positioned in these two complexes. In CaM-CaMBD2-b, the two CaMBD2-b peptides are seen at both sides of the S-shaped CaM, and they are completely separated from each other (Figures 1A and 1B). In contrast, the two CaMBD2-a peptides are much closer to each other and are wrapped around by CaM (Figures 1C and 1D; also see Figure 3, shown later).

The most intriguing and unexpected observation is that all four EF hands of CaM in the CaM-CaMBD2-b complex are occupied by Ca^{2+} ions (Figure 1). This is in striking contrast to that of the CaM-CaMBD2-a complex, in which the CaM C-lobe is Ca^{2+}-free (Figure 1) (Schumacher et al., 2001). It has been suggested that the CaM C-lobe in the CaM-CaMBD2-a complex might adopt a semiopen configuration that could contribute to the failure of the C-lobe to bind Ca^{2+} (Schumacher et al., 2004). However, structural comparison shows that the CaM C-lobe from CaM-CaMBD2-a is more likely in an open configuration, in which helices VI and VII are completely separated from helices V and VIII, similar to the CaM C-lobe from either CaM-CaMBD2-b or CaM-edema factor, both of which are Ca^{2+}-bound in their CaM C-lobes (Figures S1F and S1G). While differences can be seen in the four helices of the CaM C-lobe between CaM-CaMBD2-b and CaM-CaMBD2-a, more significant changes are observed in their loop regions, where the EF hands reside (Figure S1F). Failure to bind Ca^{2+} is also reported for the EF hands of the CaM N-lobe of the CaM-edema factor complex (Figure S1E).

CaM-CaMBD2-b Differs from CaM-CaMBD2-a in Solution

We first sought to determine whether, like CaM-CaMBD2-a (Schumacher et al., 2001), the CaM-CaMBD2-b complex would adopt a 2×2 configuration in solution in the presence of Ca^{2+}. Sedimentation equilibrium (SE) experiments were performed for both CaM-CaMBD2-b and CaM-CaMBD2-a with or without Ca^{2+}. Without Ca^{2+} (Figures 2A and 2B), the molecular mass is 28.5 ± 0.7 kDa (mean ± SD) for CaM-CaMBD2-b and 24.9 ± 2.0 kDa for CaM-CaMBD2-a, which is very close to the predicted molecular mass of a 1×1 complex, 29.3 kDa and 28.9 kDa, respectively. In the presence of Ca^{2+}, the molecular mass is doubled to 61.1 ± 1.6 kDa for CaM-CaMBD2-b and 55.8 ± 1.0 kDa for CaM-CaMBD2-a, indicating that Ca^{2+} promotes formation of a 2×2 complex in solution (Figures 2C and 2D). The SE results agree with previous reports for CaM-CaMBD2-a, which also show that, without Ca^{2+}, the CaM-CaMBD interaction

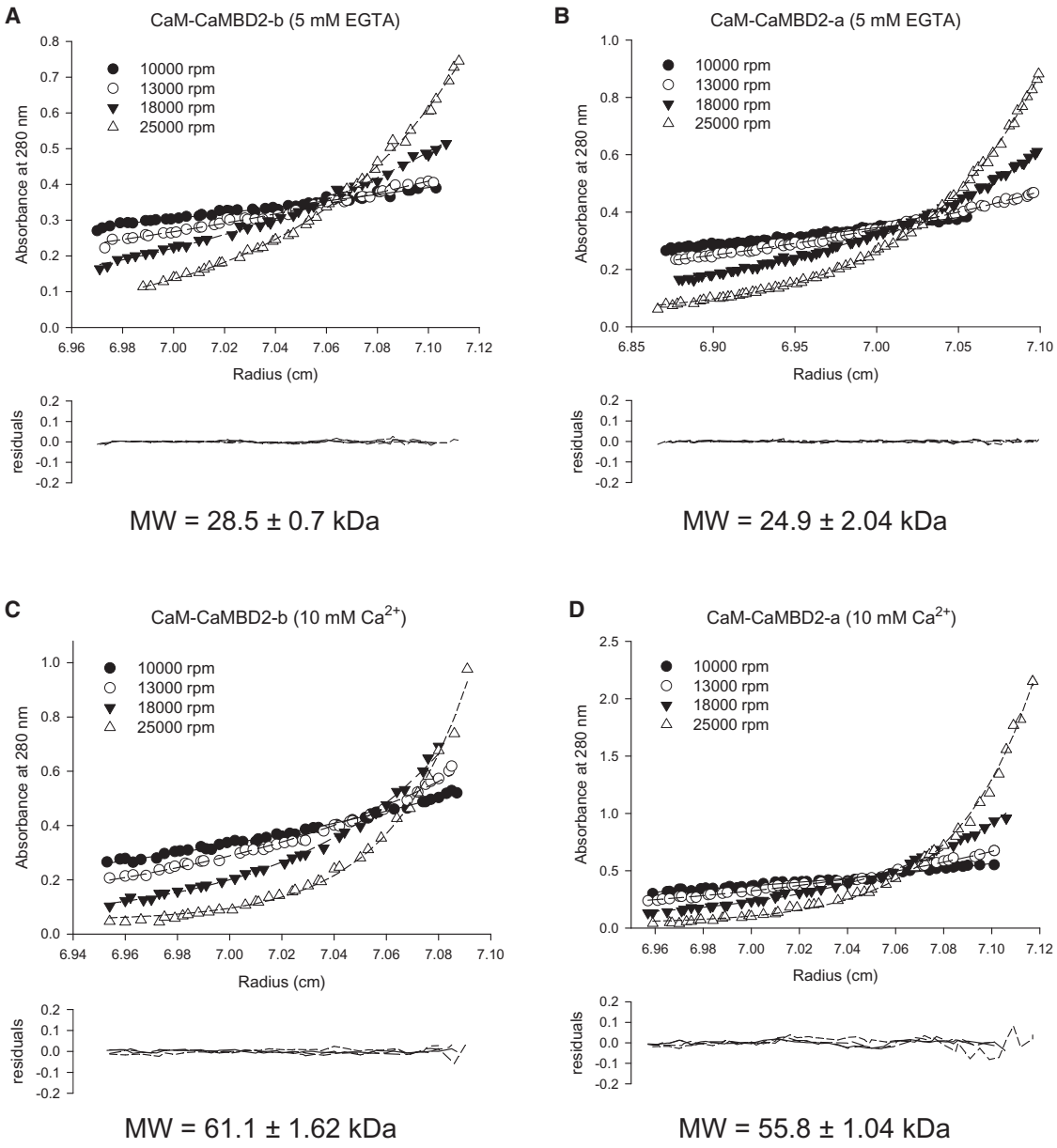

Figure 2. Ca^{2+} Promotes Formation of a 2×2 Complex for Both CaM-CaMBD2-a and CaM-CaMBD2-b in Solution

(A and B) A 1×1 complex of CaM-CaMBD2-a and CaM-CaMBD2-b in the absence of Ca^{2+}. Upper panels show raw SE data at different centrifugation speeds (indicated with four different symbols). Curves indicate fit of the raw data to a single-component model using Sedphat. Lower panels show residuals of the fit. Without Ca^{2+}, both CaM-CaMBD2-a and CaM-CaMBD2-b are 1×1, with a predicted molecular mass of 28.9 kDa and 29.3 kDa, respectively.

(C and D) A 2×2 complex of CaM-CaMBD2-a and CaM-CaMBD2-b in the presence of Ca^{2+}. Upper panels show raw SE data (symbols) with fit to a single-component model (curves), and lower panels show residuals of the fit. Ca^{2+} promotes formation of a 2×2 complex for both CaM-CaMBD2-a and CaM-CaMBD2-b with a predicted molecular mass of 57.8 kDa and 58.6 kDa, respectively.

occurs at an interface different from that in the presence of Ca^{2+} (Schumacher et al., 2004; Schumacher et al., 2001).

We then turned our attention to whether both CaM complexes might be different from each other when in solution. The structures predict that formation of the CaM-CaMBD2-b complex is a much simpler process, involving primarily the interaction between CaM and the CaMBD2-b peptide (Figure 3A). In contrast, formation of the CaM-CaMBD2-a complex includes not only the CaM-CaMBD2-a interaction but also the extensive interactions along the longer helices of two CaMBD2-a (Figure 3B). The interactions between two CaMBD2-a peptides are quite substantial, with the total surface area of 1,208 $Å^2$, compared to 1,174 $Å^2$ for the CaM-CaMBD2-a interaction at the N-lobe and 1,149 $Å^2$ for the CaM-CaMBD2-a interaction at the C-lobe. Thus, formation of the CaM-CaMBD2-a complex in the presence of Ca^{2+} undergoes a thermodynamically more complex process than that of the CaM-CaMBD2-b complex.

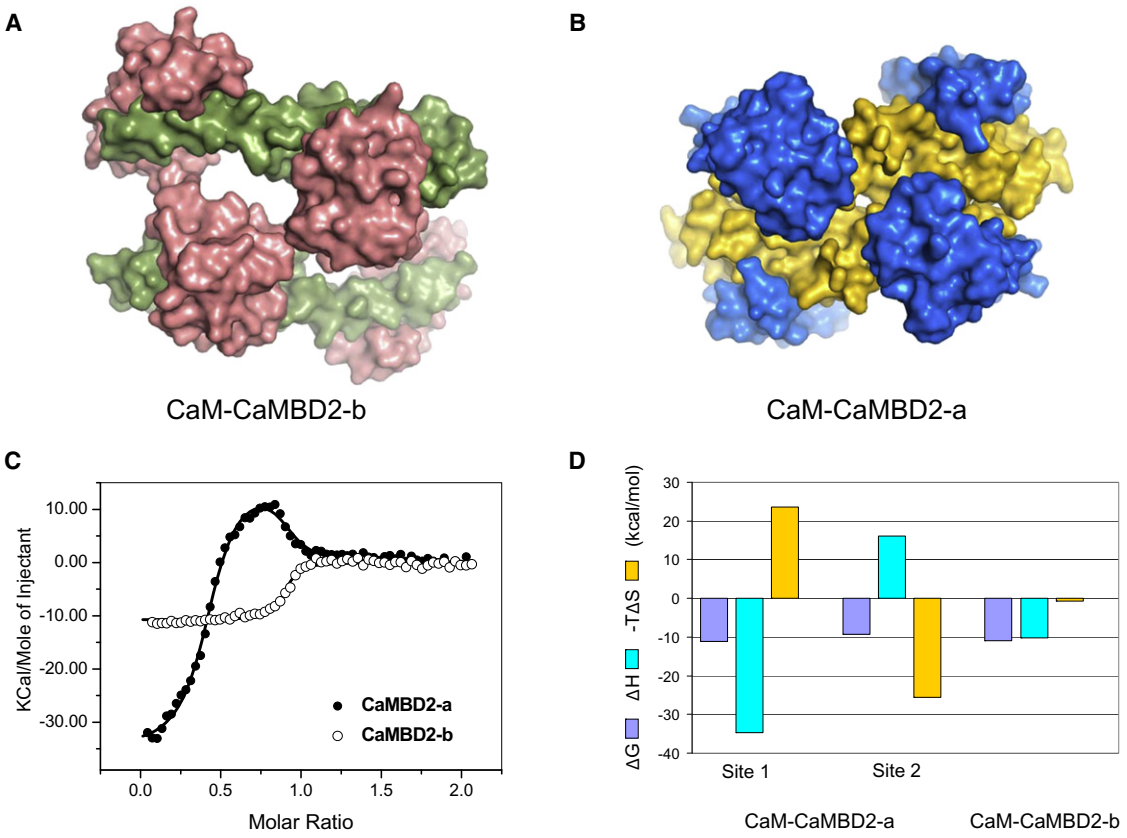

Figure 3. Different Thermodynamic Profiles for CaM-CaMBD2-b and CaM-CaMBD2-a

(A) Surface representation of the CaM-CaMBD2-b complex. CaMBD2-b (in green) interacts with CaM (in salmon pink) only at both the N- and C-lobes. There is no physical contact between the CaMBD2-b peptides.

(B) Surface representation of the CaM-CaMBD2-a complex. The CaMBD2-a peptides (in gold) form extensive contacts with CaM (in blue) as well as between themselves.

(C) Results of ITC experiments. Ca^{2+}-bound CaM was titrated into either CaMBD2-a or CaMBD2-b. For CaM-CaMBD2-a, a two-site model is required to fit the data (smooth line). On the other hand, a single-site model can adequately fit the data, and use of the two-site model did not statistically improve the fitting.

(D) Thermodynamic profiles for formation of the CaM-CaMBD2-a and CaM-CaMBD2-b complexes. Plotted are the Gibbs free energy (ΔG), enthalpy (ΔH), and entropy (−TΔS) for formation of both CaM-CaMBD2-a and CaM-CaMBD2-b. ΔG is calculated from ΔH and TΔS (Table S1), which were determined by ITC at 20°C (ΔG = ΔH − TΔS).

See also Figure S2 and Table S1.

Isothermal titration calorimetry (ITC) was used to examine the thermodynamic profiles associated with formation of the 2×2 complex of CaM-CaMBD2-b or CaM-CaMBD2-a. For both complexes, changes in heats become minuscule when the molar ratio of CaM/CaMBD approaches 1, indicating that formation of the 2×2 complex has been completed (Figures 3C and S2). Formation of the CaM-CaMBD2-b complex shows a sigmoidal relationship of the heat evolved versus the molar ratio of CaM/CaMBD2-b, which is well modeled by a single-binding-site isotherm (smooth curve; Figures 3C and S2; Table S1). In contrast, formation of the CaM-CaMBD2-a complex produces a biphasic change in heats, which is best fitted by a two-binding-site model (smooth curve; Figures 3C and S2; Table S1). Analyses show that, for CaM-CaMBD2-a, the rising phase is enthalpically favored (ΔH_1 = −34.73 ± 0.96 kcal/mol), whereas the declining phase is entropy driven (ΔS_2 = 87.2 ± 1.98 cal/mol/K). Despite dramatic differences in ΔH and TΔS, the Gibbs free energy (ΔG) for formation of CaM-CaMBD2-a is essentially the same as that of CaM-CaMBD2-b (Figure 3D). Previous studies on other CaM complexes have shown that CaM has the same affinity for different CaM-target proteins despite differences in their thermodynamics for formation of these CaM complexes (e.g., Frederick et al., 2007). Thus, in the presence of Ca^{2+}, formation of CaM-CaMBD2-a and CaM-CaMBD2-b undergoes different thermodynamic processes (ΔH and −TΔS, respectively, in Figure 3D), indicating that, in solution, these two CaM complexes are different from each other. Furthermore, in the presence of Ca^{2+}, CaM has essentially the same affinities for both CaMBD2-a and CaMBD2-b (ΔG in Figure 3D).

Structural Plasticity in the CaM Hydrophobic Binding Interfaces

In CaM-CaMBD2-b, the three additional amino acids, ARK, do not directly interact with CaM at its hydrophobic interfaces (Figure 1A). How can insertion of ARK in CaMBD2-b produce

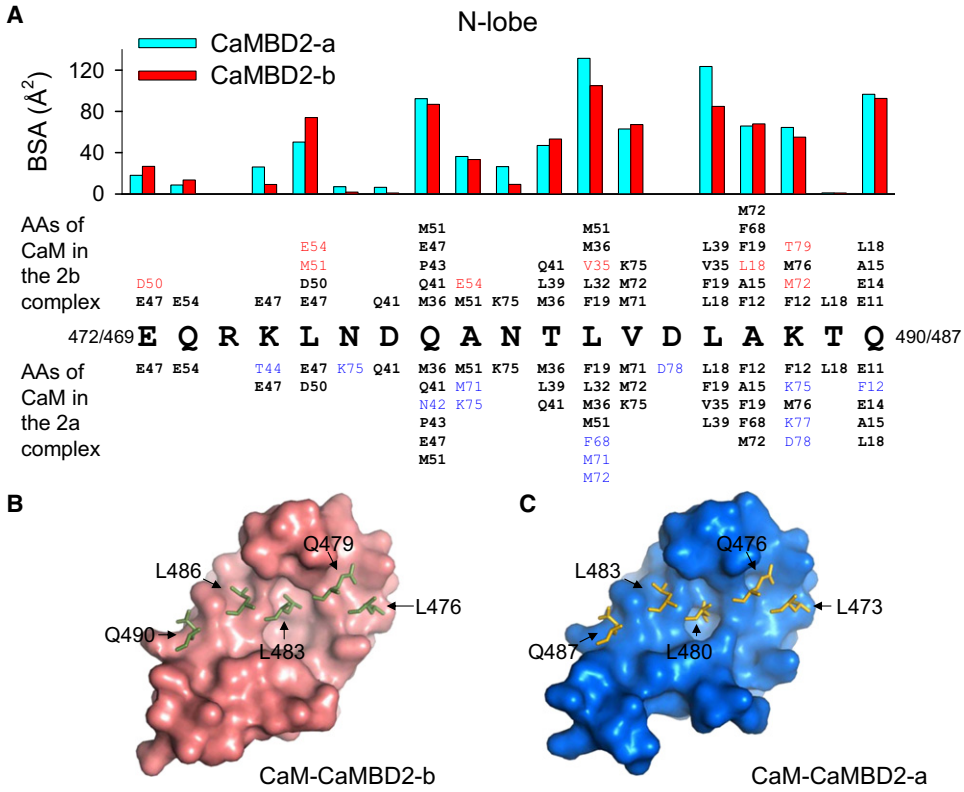

Figure 4. Interactions of CaM and CaMBDs at the CaM N-Lobe

(A) Amino acid residues involved in formation of CaM-CaMBD2-b and CaM-CaMBD2-a with Ca^{2+}. Buried surface area (BSA, bar graphs) identifies key residues in CaMBD2-b and CaMBD2-a which interact with CaM. A C-terminal fragment, from E472/E469 to L491/L488, interacts with the CaM N-lobe. Insertion of ARK shifts the numbering by three for CaMBD2-b. Also listed are CaM residues, in a smaller typeface, that are in contacts (within a 5 Å radius) with individual CaMBD residues. Shown in red are the CaM residues that only interact with key residues in CaMBD2-b. CaM residues in cyan form contacts only with CaMBD2-a. CaM residues in a black bold typeface interact with both.

(B and C) Hydrophobic interfaces of the CaM N-lobe in complex with CaMBD2-b (B) or CaMBD2-a (C). Overlaid are key residues from CaMBD2-b or CaMBD2-a. Both N-lobes are aligned from L4 to R74, with rmsd = 0.86 Å, to create the graphs.

See also Figure S3.

such a dramatic impact on the CaM conformation? Typically, a complete α-helical turn requires 3.6 amino acid residues. Insertion of ARK produces less than one full α-helical turn (60° less) and therefore alters how CaM interacts with CaMBD2-b. Upon binding Ca^{2+}, CaM undergoes conformational changes and exposes the hydrophobic surfaces in both its N- and C-lobes that interact with target proteins (Chin and Means, 2000; Halling et al., 2005; Hoeflich and Ikura, 2002; Ishida and Vogel, 2006). Extensive structural analysis was performed to identify amino acid residues involved in formation of the CaM-CaMBD2-b and CaM-CaMBD2-a complexes.

Two peptide fragments in both CaMBD2-a and CaMBD2-b interact with the CaM hydrophobic surfaces: Fragment E469/E472 to L488/L491 (insertion of ARK shifts numbering by 3 in CaMBD2-b) interacts with the CaM N-lobe, and fragment R419 to L440 forms contacts with the CaM C-lobe. Figures 4 and 5 show the plots of buried surface area (BSA) for CaMBD residues in their interactions with CaM (bar graphs in Figures 4A and 5A), as well as lists of CaM residues, within a 5-Å radius of each CaMBD residue, that are in contact with these CaMBD residues. L480/L483, with the highest BSA, serves as the anchor residue, which interacts with the hydrophobic pocket in the N-lobe. The corresponding anchor residue interacting with the CaM C-lobe is L428. Clearly, the same set of key residues in CaMBD interacts with CaM in formation of both CaM-CaMBD2-b and CaM-CaMBD2-a.

The hydrophobic interfaces in the CaM N- and C-lobes that interact with target proteins are formed by amino acid residues, particularly methionines, from all four helices of each lobe. Hydrophobic pockets, which harbor the anchor residues from CaMBD, are thought to consist primarily of FLMM, F19, L32, M51, and M71 at the N-lobe and F92, L105, M124, and M144 at the C-lobe (Ataman et al., 2007). In both CaM-CaMBD2-a and CaM-CaMBD2-b, the hydrophobic pocket at the N-lobe is made primarily of F19, L32, M36, and M51 (Figure 3A). Overall, a similar set of CaM residues contributes to formation of the hydrophobic interface at the N-lobe to interact with CaMBD2-b or CaMBD2-a in the presence of Ca^{2+}. The CaM N-lobe hydrophobic interfaces from CaM-CaMBD2-b and CaM-CaMBD2-a share similar surface topology (Figures 4B, 4C, and S3).

The hydrophobic surfaces in the CaM C-lobe vary greatly between the CaM-CaMBD2-b and CaM-CaMBD2-a complexes, and there is very little overlap between the CaM residues that contact a given target amino acid residue from CaMBD2-a or

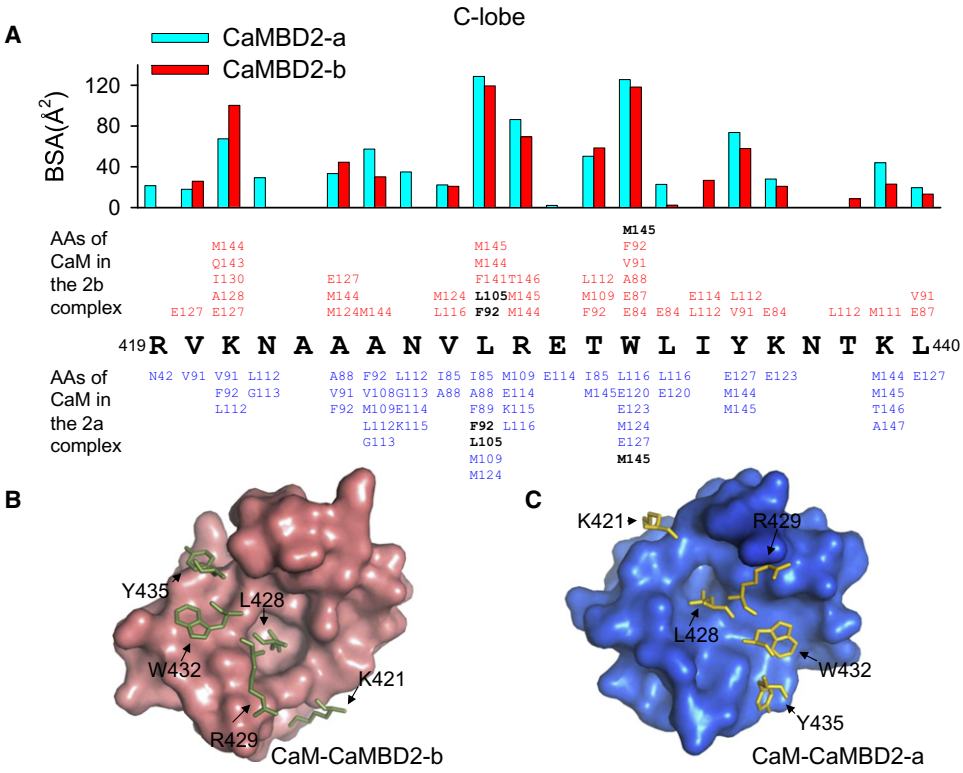

Figure 5. Interactions of CaM and CaMBDs at the CaM C-Lobe

(A) Amino acid residues involved in formation of CaM-CaMBD2-b and CaM-CaMBD2-a in the presence of Ca^{2+}, similar to descriptions in Figure 3. An N-terminal fragment, from R419 to L440, interacts with the CaM C-lobe.

(B and C) Hydrophobic interfaces of the CaM C-lobe in complex with CaMBD2-b (B) or CaMBD2-a (C). Both C-lobes are aligned from I85 to T146, with rmsd = 2.53 Å, to create the graphs.

See also Figure S4.

CaMBD2-b (Figure 5A). In the CaM-CaMBD2-b complex, the CaM C-lobe hydrophobic pocket includes F92, L105, F141, M144, and M145, while the corresponding hydrophobic pocket in CaM-CaMBD2-a is made up of I85, A88, F89, F92, L105, V108, M109, and M124 (Figures S4A and S4B). Consequently, the location of the hydrophobic pocket at the C-lobe changes significantly (Figures 5B and 5C). Another example is the hydrophobic surface for W432 from CaMBD, which interacts primarily with helix V in CaM-CaMBD2-b instead of helix VII in CaM-CaMBD2-a (Figures S4C and S4D). Thus, substantial rearrangement of the CaM C-lobe hydrophobic interface takes place, depending on which CaMBD is complexed with CaM.

Effects of CaM Target Proteins on the Conformation of Individual EF Hands in CaM

Comparison of the structures of two CaM complexes demonstrates that both CaMBD2-b and CaMBD2-a produce significant impact on the conformation of CaM, in particular, rearrangement of the hydrophobic interface at the C-lobe. In contrast, such rearrangement of the hydrophobic interface is minimal at the N-lobe. We next sought to determine whether rearrangement of the hydrophobic interfaces in the CaM C-lobe affects the conformation of the EF hands, which might provide explanations as to why the CaM C-lobe of the CaM-CaMBD2-a complex fails to bind Ca^{2+}. A canonical EF hand includes six Ca^{2+}-coordinating amino acid residues, located in the loop region and arranged as follows: 1(+X), 3(+Y), 5(+Z), 7(−X), 9(−Y), and 12(−Z) (Figure S5) (Gifford et al., 2007).

In Figure 6, the loop region of each CaM EF hand in our structure is superimposed and compared to that of the CaM-CaMBD2-a or CaM-edema factor complex. For the N-lobe, where EF hands bind Ca^{2+} ions in both CaM-CaMBD2-a and CaM-CaMBD2-b, the loop structure matches well for both EF hand 1 (rmsd = 0.26 Å) and EF hand 2 (rmsd = 0.46 Å; Figure 6A). On the other hand, EF hand 3 and EF hand 4 of the CaM C-lobe display significant structural differences between CaM-CaMBD2b and CaM-CaMBD2-a (rmsds = 1.28 Å and 1.67 Å, respectively) (Figure 6B). If the comparison includes side chains, the differences become even more significant, with rmsds of 1.96 Å for EF hand 3 and 2.46 Å for EF hand 4. The most significant differences lie with the glutamate residue at position 12(−Z) of the EF hand, E104 and E140 (Figure 6B). In CaM-CaMBD2-a, both E104 and E140 point away from the Ca^{2+} coordination sphere. Significant differences are also observed at position 1(+X), D93 and D129, and at position 3(+Z), D95 and D131. Analysis shows that the structural differences at EF hand 3 and EF hand 4 are not caused by crystal packing.

We further compared the structures of EF hands in CaM-CaMBD2-b to those of the CaM-edema factor complex (1K90), which fail to bind Ca^{2+} at the CaM N-lobe (Drum et al., 2002).

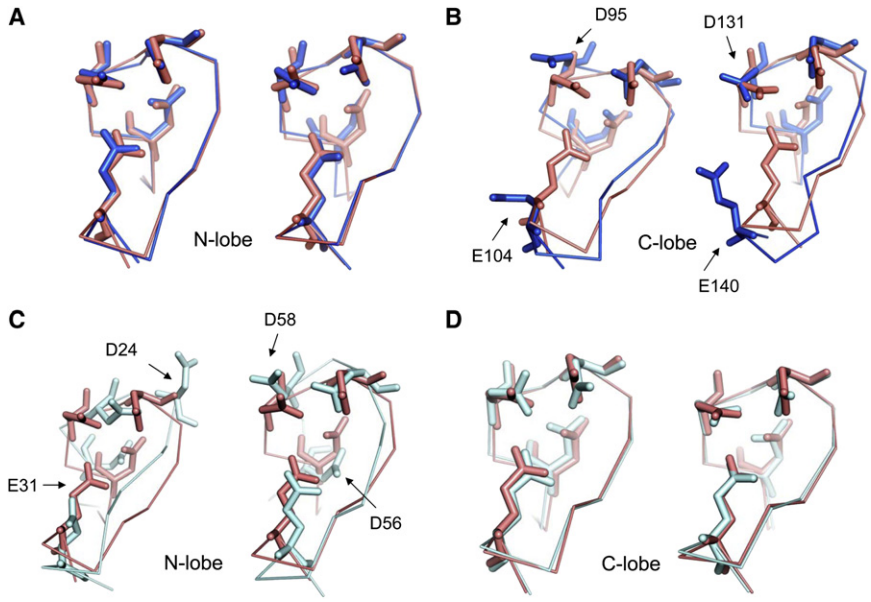

Figure 6. Conformational Plasticity of the CaM EF Hands

(A and B) Structures of EF hands from CaM-CaMBD2-b (in salmon pink) and CaM-CaMBD2-a (in blue). EF hands 1 and 2 are aligned from D20 to E31 and D56 to E67, respectively. EF hands 3 and 4 are aligned from D93 to E104 and D129 to E140, respectively. Side chains at positions 7 and 9 are not shown.

(C and D) Structures of EF hands from CaM-CaMBD2-b (in salmon pink) and the CaM-edema factor (1K90, in pale cyan). Significant differences exist in the structures of EF hands 1 and 2 but not EF hands 3 and 4. Side chains at positions 7 and 9 are not shown.

See also Figure S5.

As expected, the conformation of EF hand 1 and EF hand 2 in 1K90 is dramatically different from that of our structure (rmsds = 2.08 Å and 1.68 Å, respectively) (Figure 6C). Several key residues in both EF hand 1 and EF hand 2 of 1K90 show significantly altered spatial orientations, including D24, E31, D56, and D58. On the other hand, there is little difference at EF hand 3 and EF hand 4 of the CaM C-lobe between CaM-CaMBD2-b and the CaM-edema factor complex (Figure 6D). Thus, in CaM-CaMBD2-a, failure of binding to Ca^{2+} at the CaM C-lobe results primarily from altered conformations of EF hand 3 and EF hand 4 as a consequence of rearrangement of helices V, VI, VII, and VIII. CaMBD2-b, on the other hand, interacts with a different hydrophobic interface at the CaM C-lobe and restores the ability of EF hand 3 and EF hand 4 to bind Ca^{2+}.

CaM as a Dynamic Ca^{2+} Sensor

Our recent work has shown that SK2-b is less sensitive to Ca^{2+} for its activation (L.H. and J.F.Z., unpublished data). While differences in structures between the two CaM complexes may provide a plausible explanation, structures alone cannot rule out other potential scenarios. Binding assays were performed using AEDANS-labeled CaM(T34C or T110C), and CaMBD2-a or CaMBD2-b at different Ca^{2+} concentrations to examine the interactions between CaM and CaMBDs. The fluorescence emission intensity increases with Ca^{2+} concentrations in formation of both the CaM-CaMBD2-a and CaM-CaMBD2-b complexes (Figure S6). There is, however, a significant rightward shift of the dose-response curve for the Ca^{2+}-dependent formation of the CaM-CaMBD2-b complex (Figure 7A). The apparent K_d for Ca^{2+} is increased from 0.53 ± 0.04 μM (n = 7) for formation of CaM-CaMBD2-a to 1.18 ± 0.10 μM (n = 4) for that of CaM-CaMBD2-b ($p < 0.001$, Figure 7B); this suggests that CaM, when complexed with CaMBD2-b, may have reduced its affinity for Ca^{2+}. The Hill coefficient is 1.13 ± 0.04 (n = 7) for CaM-CaMBD2-a and 2.05 ± 0.18 (n = 4) for CaM-CaMBD2-b. Identical results were obtained with CaM(T110C).

However, such a shift in Ca^{2+}-dependent formation of the CaM-CaMBD2-b complex could also result from a reduction of the affinity of Ca^{2+}-bound CaM for CaMBD2-b (Figure S6A). Additional binding assays were performed to test such a possibility with or without Ca^{2+}. At a saturating Ca^{2+} concentration of 10 μM (Figure 7A), the fluorescence intensity of CaM(T34C) increases with the peptide concentrations of both CaMBD2-a and CaMBD2-b (Figure 7C). There is no difference in the EC_{50} for formation of either CaM-CaMBD2-a (0.15 ± 0.02 μM) or CaM-CaMBD2-b (0.18 ± 0.01 μM; n = 3, p = 0.318), suggesting that CaM, once Ca^{2+}-bound, has the same affinity for both CaMBD2-a and CaMBD2-b (Figure 7E). Identical results were obtained with CaM(T110C) instead of CaM(T34C) (data not shown). The results are consistent with our ITC data that, with saturating Ca^{2+}, CaM has the same affinity for CaMBD2-a and CaMBD2-b. Additional binding assays were performed at the Ca^{2+} concentration of 0.3 μM to further evaluate the affinity of CaM for CaMBD2-b. The fluorescence intensity of CaM(T34C) increases with CaMBD2-a, with an EC_{50} of 0.72 ± 0.09 μM, (n = 3; Figure 7E). In contrast, the CaMBD2-b peptide produces little change in the fluorescence intensity, as though there is little or no interaction between CaM and CaMBD2-b (Figure 7D). Identical results were obtained CaM(T110C). Finally, when the same binding assays were repeated without Ca^{2+}, dose-dependent changes in the fluorescence intensity with CaMBD2-b were observed with CaM(T110C) but not with CaM(T34C). CaM has the same EC_{50} for both CaMBD2-a and CaMBD2-b (data not shown). In the presence of Ca^{2+}, we never observed differential results using CaM(T34C) or CaM(T110C). This led us to conclude that increased fluorescence intensity in the presence of Ca^{2+} results from formation of a stable 2×2 complex, consistent with the SE data (Figure 2).

Collectively, the results of binding assays are consistent with the model that CaM, when complexed with CaMBD2-b, has a reduced affinity for Ca^{2+}. In principle, a reduction in Ca^{2+} affinity at either the N- or C-lobe will cause a right shift of Ca^{2+}-dependent formation of the CaM-CaMBD2-b complex (Figure 7A). Computer modeling using molecular dynamics (MD) was performed to test whether the CaM N- and C-lobes in CaM-CaMBD2-b might have different affinities for Ca^{2+}. Thermodynamic integration

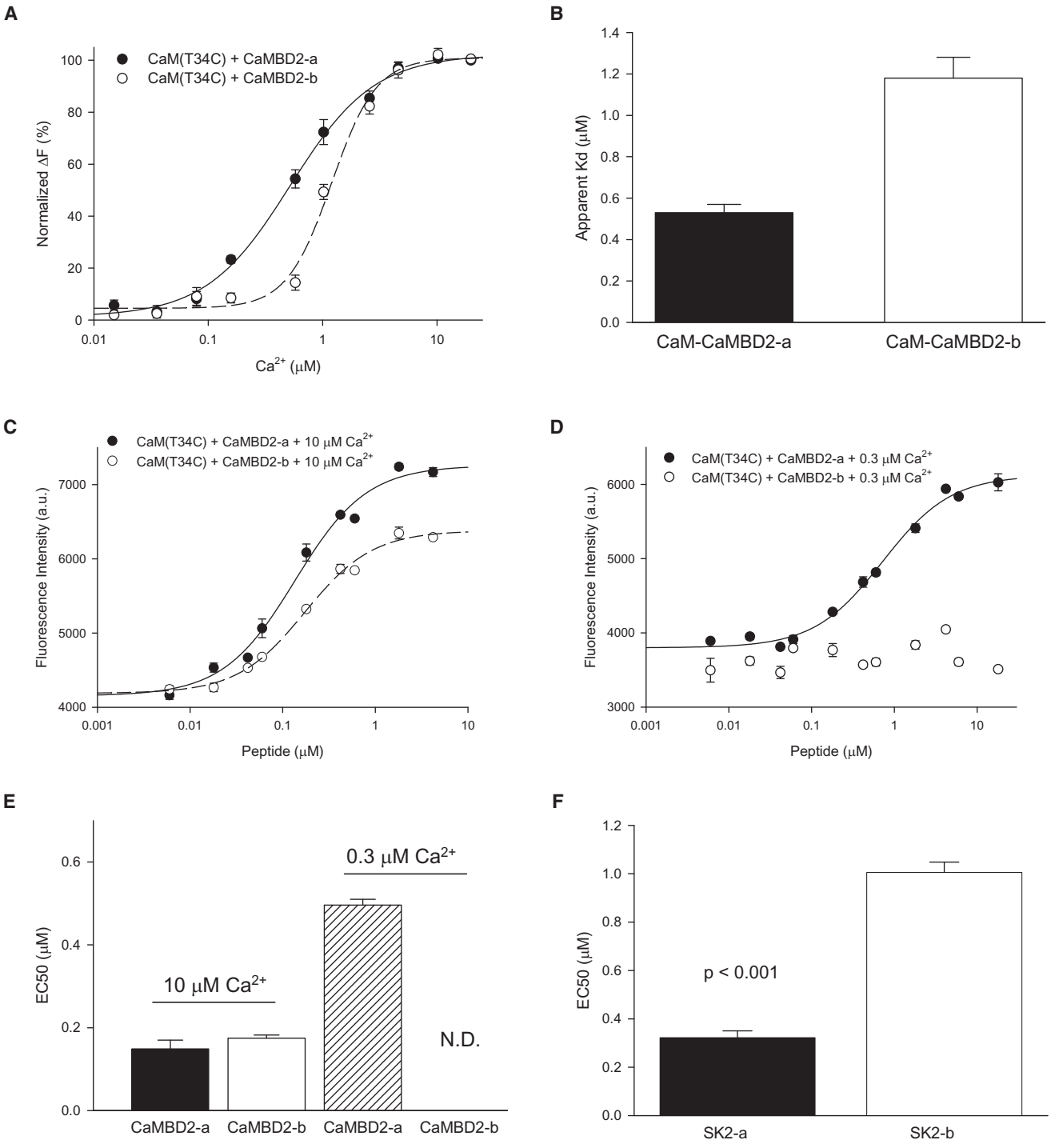

Figure 7. The CaM-CaMBD2-b Complex Has a Reduced Apparent Affinity for Ca^{2+}

(A and B) Formation of the CaM-CaMBD2-b (n = 4) complex is less sensitive to Ca^{2+}, compared to that of CaM-CaMBD2-a (n = 7). Increases in fluorescence intensity (normalized) are plotted against free Ca^{2+} concentrations (A). There is a significant reduction in the apparent K_d for Ca^{2+}, $p < 0.001$ (B). Error bars indicate mean ± SEM.

(C and D) Dose-dependent binding of CaMBD2-b (n = 3) and CaMBD2-a (n = 3) to AEDANS-labeled CaM(T34C) in the presence of 10 μM Ca^{2+} (C) or 0.3 μM Ca^{2+} (D). CaM(T110C) yielded the same results. Error bars indicate mean ± SEM.

(E) The EC_{50} of CaM for CaMBDs obtained at 10 μM or 0.3 μM Ca^{2+}. The EC_{50} of CaM for CaMBD2-b at 0.3 μM Ca^{2+} could not be determined (N.D.). Error bars indicate mean ± SEM.

(F) The EC_{50} for activation of SK2-b (n = 10) and SK2-a (n = 8) channels by Ca^{2+} from electrophysiology experiments, $p < 0.001$. Error bars indicate mean ± SEM. See also Figure S6.

calculations for the annihilation of bound Ca^{2+} were performed using all-atom, explicit-solvent MD simulations. The mean ΔΔG associated with annihilation of Ca^{2+} (N-lobe vs. C-lobe) is 18.39 ± 6.35 kcal/mol (2.72–32.88 kcal/mol; Table S2), indicating that the CaM N-lobe more stably binds Ca^{2+} than does C-lobe in the CaM-CaMBD2-b complex.

Electrophysiology experiments again confirm that SK2-b is less sensitive to Ca^{2+} for its activation compared to SK2-a. The EC_{50} for activation of SK2-b by Ca^{2+} is 1.01 ± 0.04 μM (n = 12), approximately three times higher than the EC_{50} for activation of SK2-a (0.32 ± 0.03 μM; n = 8, $p < 0.001$, Figure 7F). The magnitude of the change in EC_{50} for Ca^{2+}-dependent channel activation is comparable to that of the Ca^{2+}-dependent interaction between CaM and CaMBDs (Figure 7D). The Hill coefficient is 3.64 ± 0.28 (n = 12) for SK2-b and 3.58 ± 0.29 (n = 8) for SK2-a. This is likely due to the fact that a functional SK channel is a tetramer, and each SK channel will have four CaM molecules attached. These results show that CaM, when in complex with CaMBD2-b, has a lower affinity for Ca^{2+}, which is the primary reason that SK2-b becomes less sensitive to Ca^{2+} for its activation. Depending on the SK2 splice variant to which CaM binds, CaM changes its conformation and its affinity for Ca^{2+}, capable of responding to a much wider range of Ca^{2+} concentrations in Ca^{2+}-dependent signaling.

DISCUSSION

In this study, we show that insertion of three additional amino acid residues, ARK, in CaMBD2-b drastically alters the conformation of CaM as well as CaM's affinity for Ca^{2+} in CaM-CaMBD2-b compared to CaM-CaMBD2-a. Several key structural features contribute to such significant changes. (1) Both CaMBD2-a and CaMBD2-b form a 2×2 complex with CaM in solution (Figure 2). Without the constraint of the 2×2 configuration, CaM in CaM-CaMBD2-b will not adopt a conformation different from that of CaM-CaMBD2-a, nor will it change its affinity for Ca^{2+}. (2) Insertion of ARK rotates the downstream residues of CaMBD2-b by less than one full α-helical turn (~300°). This effectively changes the relative spatial orientations of the two fragments in CaMBD2-b that interact with the CaM N- and C-lobes. (3) The conformations of the CaM N-lobe are virtually identical in both CaM-CaMBD2-a and CaM-CaMBD2-b (Figures 1, 4, and 6). Therefore, the affinity of the CaM N-lobe for Ca^{2+} will be similar, if not identical, between the two CaM complexes. (4) The structural flexibility allows substantial conformational changes of CaM in the hydrophobic interface at the CaM C-lobe (Figures 1, 5, and 6). One important consequence is that such conformational changes restore the ability of the CaM C-lobe to bind Ca^{2+} in CaM-CaMBD2-b. Thus, the CaM C-lobe can be Ca^{2+}-bound or Ca^{2+}-free (a very low affinity for Ca^{2+}), depending on which SK2 variant peptide it interacts with (Figure 6).

Formation of the CaM-CaMBD2-b complex (2×2) becomes Ca^{2+} dependent, not only at the CaM N-lobe but also at the CaM C-lobe (Figure 8A). In contrast, for CaM-CaMBD2-a, exposure of the hydrophobic interface at the CaM C-lobe is induced primarily by CaMBD2-a, independent of Ca^{2+} (Figure 8B). It is generally thought that the CaM C-lobe has a higher affinity for Ca^{2+} than the N-lobe (Andersson et al., 1983; Crouch and Klee, 1980). When CaM is associated with its target proteins,

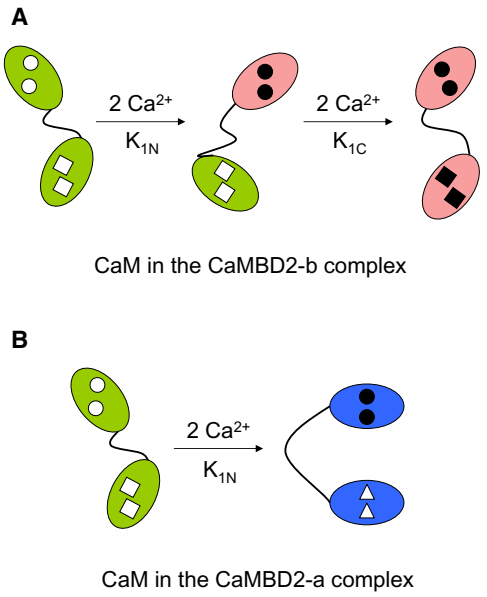

Figure 8. A Molecular Model for Changes in CaM's Affinity for Ca^{2+}, Induced by CaMBD2-b or CaMBD2-a

In the presence of Ca^{2+}, CaM forms a 2×2 complex with both CaMBD2-b and CaMBD2-a in solution. Formation of the CaM-CaMBD2-b complex in the presence of Ca^{2+} requires that both the CaM N- and C-lobes become Ca^{2+}-bound before they can interact with CaMBD2-b (A). The CaM C-lobe has a lower affinity for Ca^{2+} than the N-lobe ($K_{1C} < K_{1N}$), effectively determining the overall reduced Ca^{2+} sensitivity in formation of the 2×2 CaM-CaMBD2-b complex. In contrast, formation of the CaM-CaMBD2-a complex is Ca^{2+}-dependent at the CaM N-lobe and becomes Ca^{2+}-independent at the CaM C-lobe. (B). The open symbols represent the Ca^{2+}-free EF hands, while the filled circles and squares represent Ca^{2+}-bound EF hands. The open triangles represent EF hands that are no longer able to bind Ca^{2+}.

the affinity of CaM for Ca^{2+} becomes even higher (Peersen et al., 1997). Our results show that the opposite can happen as well. The CaM C-lobe in the CaM-CaMBD2-b complex has a lower affinity for Ca^{2+} than the N-lobe, effectively determining the overall reduced Ca^{2+} sensitivity in formation of the 2×2 CaM-CaMBD2-b complex (a rightward shift of the dose-response curve in Figure 7A).

Structural flexibility has been proposed as a mechanism through which CaM is able to interact with a variety of target proteins, even though these target proteins do not share common structural features. Globally, conformational changes of CaM include at least two major processes: (1) unwinding of the α-helix in the CaM linker region (R74 to E83) and (2) exposure of the hydrophobic interfaces at both the N- and C-lobes when CaM becomes Ca^{2+}-bound (Chin and Means, 2000; Drum et al., 2002; Fallon and Quiocho, 2003; Halling et al., 2005; Hoeflich and Ikura, 2002; Ikura et al., 1992; Ishida and Vogel, 2006; Meador et al., 1992, 1993; Mori et al., 2008; Van Petegem et al., 2005). The CaM linker region is extremely flexible. When CaM is complexed with its target proteins, the linker region often unwinds and allows CaM to wrap around the target proteins with its N- and C-lobes (Meador et al., 1992, 1993; Mori et al., 2008; Osawa et al., 1999; Van Petegem et al., 2005). Different from these previously reported structures, CaM in the CaM-CaMBD2-b complex adopts a rigid α-helical conformation in

its linker region (Figure 1). Such an extended conformation of CaM has been reported in other CaM complexes (Larsson et al., 2001; Rodríguez-Castañeda et al., 2010).

Once Ca^{2+}-bound, CaM undergoes significant conformational changes in the N- and C-lobes, adopting an open mode configuration that exposes the hydrophobic interfaces for interactions with the target proteins (Chin and Means, 2000; Halling et al., 2005; Hoeflich and Ikura, 2002; Ishida and Vogel, 2006; Meador et al., 1992, 1993; Schumacher et al., 2004). This Ca^{2+}-dependent transition from the closed mode to the open mode is key to Ca^{2+}-dependent interaction between CaM and CaM target proteins. The consensus is that exposure of the CaM hydrophobic interface results from binding of Ca^{2+} to the EF hands at both the CaM N- and C-lobes. On the other hand, the CaM C-lobe in CaM-CaMBD2-a fails to bind Ca^{2+} but nevertheless is able to expose its hydrophobic interface for its interaction with CaMBD2-a. This Ca^{2+}-independent interaction is achieved through the semiopen conformation, particularly at the CaM C-lobe (Chagot and Chazin, 2011; Swindells and Ikura, 1996; Urbauer et al., 1995). Our work shows that the hydrophobic interface at the CaM C-lobe can be made of almost entirely different sets of amino acid residues, even though the interacting amino acids on CaMBD remain the same (Figures 4 and 5), again demonstrating the structure plasticity of CaM in mediating Ca^{2+}-dependent signaling.

CaM is a dynamic Ca^{2+} sensor, capable of responding to a wide range of Ca^{2+} concentrations (e.g., 10^{-12} M–10^{-6} M) in Ca^{2+}-dependent cellular signaling (Chin and Means, 2000). Previous work on CaM-target protein complexes often used short CaMBD peptides. While valuable information has been obtained, one disadvantage of using short CaMBD peptides is that the interactions between CaM and CaMBD are greatly simplified, especially the lack of the effects of the target proteins on the conformation of CaM. The results of this study, together with the work on CaM-CaMBD2-a (1G4Y) and CaM-edema factor (1K90), demonstrate that target proteins have significant impact not only on the CaM's structure but, more important, on CaM's affinity for Ca^{2+}. For instance, CaM in the CaM-CaMBD2-a complex has lost its ability to bind Ca^{2+} at its C-lobe, while CaM in the CaM-CaMBD2-b has restored its ability to bind Ca^{2+} at its C-lobe. CaM in the CaM-edema factor complex fails to bind Ca^{2+} at its N-lobe (Drum et al., 2002). Thus, target proteins can drastically decrease, not just increase, the affinity of CaM for Ca^{2+}. Thus, changes in CaM's conformations, induced by target proteins, provide an additional mechanism that allows CaM to respond to Ca^{2+} signals of different strength, as observed in local versus global Ca^{2+} sensing at sites of Ca^{2+} entry into the cytoplasm (Dick et al., 2008; Tadross et al., 2008).

EXPERIMENTAL PROCEDURES

Protein Expression and Purification

Rat CaM cDNA was cloned into pET-28b (Novagen), expressed in *Escherichia coli* strain Rosetta2(DE3) (Novagen), and purified using a low substitution phenyl sepharose fast flow column and an AKTA purifier (GE Healthcare). The codons of the CaMBD2-b were optimized for expression in *E. coli*, and the synthetic gene was cloned into pET-28b. The sequence of the CaMBD2-b (including the His-tag) used for expression is as follows: MDTQLTKRVK NAAANVLRETWLIYKNTKLVKKIDHAKVRKHQRKFLQAIHQARKLRSVKMEQR KLNDQANTLVDLAKTQLEHHHHHH. This C-terminal His-tag fusion protein fragment was expressed, solubilized with 0.2% w/v sarkosyl, and purified on a nickel column (QIAGEN). Both CaM and CaMBD were subsequently purified using a Sephacryl S-100 high-resolution gel filtration column (GE Healthcare). The protein complex was formed by slowly adding the CaMBD2-b to CaM. The complex was then purified using the gel filtration column (GE Healthcare) pre-equilibrated in a solution with 10 mM Tris-HCl, 50 mM NaCl, and 10 mM $CaCl_2$ (pH 7.5). Fractions were collected and concentrated to 3 mM. Protein concentrations were determined by predicted extinction coefficients.

Crystallization and Structure Determination

Please see the Supplemental Experimental Procedures for details.

Sedimentation Equilibrium

SE experiments were performed as previously described (Schumacher et al., 2001). Briefly, for SE analysis of the complexes in the presence of Ca^{2+}, both protein complexes were dialyzed into a solution with 50 mM NaCl, 10 mM Tris, and 10 mM $CaCl_2$, pH 7.5. For SE analysis of the complexes in the absence of Ca^{2+}, both protein complexes were dialyzed into a solution with 50 mM NaCl, 10 mM Tris, and 5 mM EGTA, pH 7.5. Protein complexes at 30 μM loading concentration were sedimented to equilibrium at 10,000, 13,000, 18,000, and 25,000 rpm in a Beckman XL-I Analytical Ultracentrifuge using an An 50 Ti rotor. Radial absorbance scans measured at 280 nm determined the distribution of the complexes in the centrifugal field. Data analysis was performed using SEDFIT and SEDPHAT (Schuck et al., 2002). A single component model yielded the best fit to the data.

Isothermal Titration Calorimetry

For ITC experiments, CaM, CAMBD2-a, and CaMBD2-b were expressed and purified using affinity columns followed by gel filtration with the following buffer: 20 mM HEPES and 100 mM NaCl, pH 7.5. Both CaM and CaMBDs were dialyzed into the same buffer supplemented with 10 mM $CaCl_2$. CaM (90 μM) was titrated into CaMBD2-a (10 μM) or CaMBD2-b (10 μM) at 20°C using a microcalorimeter (MicroCal/GE). The injection volume was 4 μl, and the initial cell volume of CaMBDs was 1.43 ml. For data analysis, the dilution heat generated from titration of CaM into the buffer without CaMBD peptides was measured and subtracted from that with either CaMBD2-b or CaMBD2-a. There were no noticeable changes in the dilution heat. Data were fitted to standard equations in Origin 7.0 supplied by MicroCal. Identical results were obtained in three independent experiments with different batches of the purified proteins.

Fluorescence Measurements with Fluorophore-Labeled CaM

Dansyl-labeled CaM is often used to quantify the interaction between CaM and its target proteins (e.g., Zühlke et al., 1999). Dansyl labeling, however, will modify the Lys residues in CaM and potentially alter the interaction between CaM and CaMBD, since K75, K77, and K115 in CaM are clearly involved in interacting with CaMBD (Figures 4 and 5). Instead, fluorophore-labeled CaM was created by introducing a cysteine mutation in CaM (T34C or T110C), as previously described (Halling et al., 2009; Spratt et al., 2007). The fluorophore changes its fluorescence intensity in response to changes in the local environment near the fluorophore. The mutant CaM was expressed and purified as described earlier (plus 0.5 mM TCEP) and was labeled with 5-((((2-iodoacetyl) amino)ethyl)amino)naphthalene-1-sulfonic acid (AEDANS, Invitrogen). All proteins were dialyzed into the solution containing (in mM) 20 mM HEPES, 100 mM NaCl, 10 mM EGTA, 10 mM HEDTA, and 0.2 mM TCEP, pH 7.0. Binding assays were performed by mixing 0.2 μM of AEDANS-labeled CaM(T34C) or CaM(T110C) with 3 μM of either CaMBD2-a or CaMBD2-b and adding Ca^{2+} to its final free concentrations calculated with the software by Chris Patton of Stanford University (http://www.stanford.edu/~cpatton/maxc.html). The mixture was incubated for 3 hr at room temperature in dark. The fluorescence was measured using a Safire II microplate reader (Texan) with excitation at 340 nm (10 nm bandwidth) and emission between 400 and 600 nm (scanned with 20 nm bandwidth) at 28°C. The increase of fluorescence intensity, at emission of 510 nm, was plotted as a function of the free Ca^{2+} concentrations and fitted with a standard dose-response curve. In a separate experiment, AEDANS-labeled CaM (0.2 μM) was mixed with an increasing amount of CaMBDs at Ca^{2+} concentrations as indicated. Changes in the fluorescence intensity were plotted as a function of the CaMBD concentrations and fitted with a standard dose-response curve.

Electrophysiology

Please see the Supplemental Experimental Procedures for details.

Calculation of Relative Binding Affinities of the CaM N- and C-Lobes for Ca^{2+}

The CaM-CaMBD2-b crystal structure was subject to 18 ns of explicit solvent MD simulation using NAMD v2.8 (Phillips et al., 2005) and the CHARMM force field (Mackerell et al., 2004), at 298 K and 1 bar to provide an ensemble of configurations. Configurations were sampled at 4, 8, 12, and 16 ns to provide initial configurations for thermodynamic integration (TI) calculations (Frenkel and Smit, 2002). TI was performed along a discrete alchemical pathway connecting the Ca^{2+}-bound state to a Ca^{2+}-free state for two particular Ca^{2+} ions: those that bound to EF hands in the CaM N-lobe (chain A) and those that bound to EF hands in the CaM C-lobe (chain A). The TI order parameters for van der Waals and electrostatic interactions were varied from 1.0 (Ca^{2+} fully bound) to 0.0 (Ca^{2+} fully absent) according to a schedule that turns electrostatics off first before completely turning off van der Waals (see Supplemental Experimental Procedures). Numerical integration was performed using the trapezoidal rule.

Statistics

Where applicable, data are expressed as mean ± SEM. Student t tests are used for data comparison.

ACCESSION NUMBERS

The coordinates of the CaM-CaMBD2-b complex have been deposited in the Protein Data Bank under accession code 3SJQ. The accession number of the SK2-b gene is JN857942.

SUPPLEMENTAL INFORMATION

Supplemental Information includes six figures, two tables, and Supplemental Experimental Procedures and can be found with this article online at doi:10.1016/j.str.2012.03.019.

ACKNOWLEDGMENTS

The work is supported by grants from the National Institutes of Health to J.F.Z. (R01MH073060 and R01NS39355). We thank Drs. Horn, Aldrich, Levitan, Covarrubias, Root, Scott, Milev, Horne, and Armen for their encouragement and helpful discussions; Drs. Yue, Tang, and Leppla for providing plasmids of CaM mutants and edema factor; Drs. Eto and Butler for their help with fluorescence measurement; the structural facility of the Kimmel Cancer Center at Thomas Jefferson University for access of equipment in initial protein crystal screening, initial in-house X-ray diffraction, and ITC experiments; and the staff at the Beamline facility (X29A) of the Brookhaven National Laboratory for assistance with collection of X-ray diffraction data.

Received: September 9, 2011
Revised: February 20, 2012
Accepted: March 8, 2012
Published: May 8, 2012

REFERENCES

Andersson, A., Forsén, S., Thulin, E., and Vogel, H.J. (1983). Cadmium-113 nuclear magnetic resonance studies of proteolytic fragments of calmodulin: assignment of strong and weak cation binding sites. Biochemistry *22*, 2309–2313.

Ataman, Z.A., Gakhar, L., Sorensen, B.R., Hell, J.W., and Shea, M.A. (2007). The NMDA receptor NR1 C1 region bound to calmodulin: structural insights into functional differences between homologous domains. Structure *15*, 1603–1617.

Bond, C.T., Maylie, J., and Adelman, J.P. (2005). SK channels in excitability, pacemaking and synaptic integration. Curr. Opin. Neurobiol. *15*, 305–311.

Chin, D., and Means, A.R. (2000). Calmodulin: a prototypical calcium sensor. Trends Cell Biol. *10*, 322–328.

Chagot, B., and Chazin, W.J. (2011). Solution NMR structure of Apo-calmodulin in complex with the IQ motif of human cardiac sodium channel NaV1.5. J. Mol. Biol. *406*, 106–119.

Clapham, D.E. (2007). Calcium signaling. Cell *131*, 1047–1058.

Crouch, T.H., and Klee, C.B. (1980). Positive cooperative binding of calcium to bovine brain calmodulin. Biochemistry *19*, 3692–3698.

Deisseroth, K., Heist, E.K., and Tsien, R.W. (1998). Translocation of calmodulin to the nucleus supports CREB phosphorylation in hippocampal neurons. Nature *392*, 198–202.

Dick, I.E., Tadross, M.R., Liang, H., Tay, L.H., Yang, W., and Yue, D.T. (2008). A modular switch for spatial Ca2+ selectivity in the calmodulin regulation of CaV channels. Nature *451*, 830–834.

Drum, C.L., Yan, S.-Z., Bard, J., Shen, Y.-Q., Lu, D., Soelaiman, S., Grabarek, Z., Bohm, A., and Tang, W.-J. (2002). Structural basis for the activation of anthrax adenylyl cyclase exotoxin by calmodulin. Nature *415*, 396–402.

Faber, E.S.L. (2009). Functions and modulation of neuronal SK channels. Cell Biochem. Biophys. *55*, 127–139.

Fallon, J.L., and Quiocho, F.A. (2003). A closed compact structure of native $Ca^{(2+)}$-calmodulin. Structure *11*, 1303–1307.

Frederick, K.K., Marlow, M.S., Valentine, K.G., and Wand, A.J. (2007). Conformational entropy in molecular recognition by proteins. Nature *448*, 325–329.

Frenkel, D., and Smit, B. (2002). Understanding molecular simulation (San Diego, CA: Academic Press).

Gifford, J.L., Walsh, M.P., and Vogel, H.J. (2007). Structures and metal-ion-binding properties of the Ca^{2+}-binding helix-loop-helix EF-hand motifs. Biochem. J. *405*, 199–221.

Halling, D.B., Aracena-Parks, P., and Hamilton, S.L. (2005). Regulation of voltage-gated Ca^{2+} channels by calmodulin. Sci. STKE *2005*, re15.

Halling, D.B., Georgiou, D.K., Black, D.J., Yang, G., Fallon, J.L., Quiocho, F.A., Pedersen, S.E., and Hamilton, S.L. (2009). Determinants in CaV1 channels that regulate the Ca^{2+} sensitivity of bound calmodulin. J. Biol. Chem. *284*, 20041–20051.

Hoeflich, K.P., and Ikura, M. (2002). Calmodulin in action: diversity in target recognition and activation mechanisms. Cell *108*, 739–742.

Ikura, M., Clore, G.M., Gronenborn, A.M., Zhu, G., Klee, C.B., and Bax, A. (1992). Solution structure of a calmodulin-target peptide complex by multidimensional NMR. Science *256*, 632–638.

Ishida, H., and Vogel, H.J. (2006). Protein-peptide interaction studies demonstrate the versatility of calmodulin target protein binding. Protein Pept. Lett. *13*, 455–465.

Köhler, M., Hirschberg, B., Bond, C.T., Kinzie, J.M., Marrion, N.V., Maylie, J., and Adelman, J.P. (1996). Small-conductance, calcium-activated potassium channels from mammalian brain. Science *273*, 1709–1714.

Kranz, J.K., Lee, E.K., Nairn, A.C., and Wand, A.J. (2002). A direct test of the reductionist approach to structural studies of calmodulin activity. J. Biol. Chem. *277*, 16351–16354.

Larsson, G., Schleucher, J., Onions, J., Hermann, S., Grundström, T., and Wijmenga, S.S. (2001). A novel target recognition revealed by calmodulin in complex with the basic helix–loop–helix transcription factor SEF2-1/E2-2. Protein Sci. *10*, 169–186.

Mackerell, A.D., Jr., Feig, M., and Brooks, C.L., 3rd. (2004). Extending the treatment of backbone energetics in protein force fields: limitations of gas-phase quantum mechanics in reproducing protein conformational distributions in molecular dynamics simulations. J. Comput. Chem. *25*, 1400–1415.

McLaughlin, S., and Murray, D. (2005). Plasma membrane phosphoinositide organization by protein electrostatics. Nature *438*, 605–611.

Meador, W.E., Means, A.R., and Quiocho, F.A. (1992). Target enzyme recognition by calmodulin: 2.4 A structure of a calmodulin-peptide complex. Science *257*, 1251–1255.

Meador, W.E., Means, A.R., and Quiocho, F.A. (1993). Modulation of calmodulin plasticity in molecular recognition on the basis of x-ray structures. Science *262*, 1718–1721.

Mori, M.X., Vander Kooi, C.W., Leahy, D.J., and Yue, D.T. (2008). Crystal structure of the CaV2 IQ domain in complex with Ca2+/calmodulin: high-resolution mechanistic implications for channel regulation by Ca2+. Structure *16*, 607–620.

Osawa, M., Tokumitsu, H., Swindells, M.B., Kurihara, H., Orita, M., Shibanuma, T., Furuya, T., and Ikura, M. (1999). A novel target recognition revealed by calmodulin in complex with Ca2+-calmodulin-dependent kinase kinase. Nat. Struct. Biol. *6*, 819–824.

Peersen, O.B., Madsen, T.S., and Falke, J.J. (1997). Intermolecular tuning of calmodulin by target peptides and proteins: differential effects on Ca2+ binding and implications for kinase activation. Protein Sci. *6*, 794–807.

Phillips, J.C., Braun, R., Wang, W., Gumbart, J., Tajkhorshid, E., Villa, E., Chipot, C., Skeel, R.D., Kalé, L., and Schulten, K. (2005). Scalable molecular dynamics with NAMD. J. Comput. Chem. *26*, 1781–1802.

Rodríguez-Castañeda, F., Maestre-Martínez, M., Coudevylle, N., Dimova, K., Junge, H., Lipstein, N., Lee, D., Becker, S., Brose, N., Jahn, O., et al. (2010). Modular architecture of Munc13/calmodulin complexes: dual regulation by Ca^{2+} and possible function in short-term synaptic plasticity. EMBO J. *29*, 680–691.

Schuck, P., Perugini, M.A., Gonzales, N.R., Howlett, G.J., and Schubert, D. (2002). Size-distribution analysis of proteins by analytical ultracentrifugation: strategies and application to model systems. Biophys. J. *82*, 1096–1111.

Schumacher, M.A., Rivard, A.F., Bächinger, H.P., and Adelman, J.P. (2001). Structure of the gating domain of a Ca2+-activated K+ channel complexed with Ca2+/calmodulin. Nature *410*, 1120–1124.

Schumacher, M.A., Crum, M., and Miller, M.C. (2004). Crystal structures of apocalmodulin and an apocalmodulin/SK potassium channel gating domain complex. Structure *12*, 849–860.

Spratt, D.E., Taiakina, V., Palmer, M., and Guillemette, J.G. (2007). Differential binding of calmodulin domains to constitutive and inducible nitric oxide synthase enzymes. Biochemistry *46*, 8288–8300.

Stocker, M. (2004). $Ca(^{2+})$-activated K^{+} channels: molecular determinants and function of the SK family. Nat. Rev. Neurosci. *5*, 758–770.

Swindells, M.B., and Ikura, M. (1996). Pre-formation of the semi-open conformation by the apo-calmodulin C-terminal domain and implications binding IQ-motifs. Nat. Struct. Biol. *3*, 501–504.

Tadross, M.R., Dick, I.E., and Yue, D.T. (2008). Mechanism of local and global Ca2+ sensing by calmodulin in complex with a Ca2+ channel. Cell *133*, 1228–1240.

Urbauer, J.L., Short, J.H., Dow, L.K., and Wand, A.J. (1995). Structural analysis of a novel interaction by calmodulin: high-affinity binding of a peptide in the absence of calcium. Biochem *34*, 8099–8109.

Van Petegem, F., Chatelain, F.C., and Minor, D.L., Jr. (2005). Insights into voltage-gated calcium channel regulation from the structure of the CaV1.2 IQ domain-Ca2+/calmodulin complex. Nat. Struct. Mol. Biol. *12*, 1108–1115.

Wayman, G.A., Lee, Y.-S., Tokumitsu, H., Silva, A.J., and Soderling, T.R. (2008). Calmodulin-kinases: modulators of neuronal development and plasticity. Neuron *59*, 914–931.

Xia, X.M., Fakler, B., Rivard, A., Wayman, G., Johnson-Pais, T., Keen, J.E., Ishii, T., Hirschberg, B., Bond, C.T., Lutsenko, S., et al. (1998). Mechanism of calcium gating in small-conductance calcium-activated potassium channels. Nature *395*, 503–507.

Zühlke, R.D., Pitt, G.S., Deisseroth, K., Tsien, R.W., and Reuter, H. (1999). Calmodulin supports both inactivation and facilitation of L-type calcium channels. Nature *399*, 159–162.